

Control System Design Implementation and Preliminary Demonstration for a Tendon-Actuated Lightweight In-Space MANipulator (TALISMAN)

Erik E. Komendera * and William R. Doggett † and John T. Dorsey ‡

NASA Langley Research Center, Hampton, VA 23681, USA

Thomas J. Debus § and Kris Holub ¶

and Sean P. Dougherty ||

MDA US Systems, LLC, Boulder, CO 80301, USA

Satellite servicing is a high priority task for NASA and the space industry, addressing the needs of a variety of missions, and potentially lowering the overall cost of missions through refurbishment and reuse. However, the ability to service satellites is severely limited by the lack of long reach manipulation capability and inability to launch new devices due the end of the Space Transport System, or Space Shuttle Program. This paper describes the design and implementation of a control system for a Tendon-Actuated Lightweight In-Space MANipulator (TALISMAN), including; defining the forward and inverse kinematics, endpoint velocity to motor velocity, required cable tensions, and a proportional-integral-derivative (PID) controller. The tensions and velocities necessary to maneuver and capture small and large payloads are also discussed. To demonstrate the utility of the TALISMAN for satellite servicing, this paper also describes a satellite servicing demonstration using two TALISMAN prototypes to grasp and inspect a satellite mockup. Potential avenues for improving the control system are discussed.

Nomenclature

a_i	Acceleration at joint i ($\frac{m}{s^2}$)
β	Ratio of coasting phase to acceleration phase in motion planning
c_β	Intermediate variable for inverse kinematics calculation
C_1, C_2, C_3	Intermediate variables for Inverse Jacobian calculation
c_3	Intermediate variable for inverse kinematics calculation
d_i	Length of the i -th link (m)
d_t	Intermediate variable for inverse kinematics calculation
DOF	Degrees of freedom
$\frac{dZ_{i,c,MAX}}{dt}$	Maximum cable length change rate at joint i ($\frac{m}{s}$)
$\frac{d^2\theta_{i,MAX}}{dt^2}$	Maximum angular acceleration at joint i ($\frac{\text{rad}}{s^2}$)
$\frac{d\theta_{i,M,MAX}}{dt}$	Maximum motor angular velocity at joint i ($\frac{\text{rad}}{s}$)
e_{T_i}	Error in tension in the variable tension cable, used in PID control (N)
e_{θ_i}	Error in angle, used in PID control (rad)
f_c	Fraction planned motion time spent in coasting phase
F_{tip}	Force applied at the endpoint (N)

*Research Aerospace Engineer, Structural Mechanics and Concepts Branch, Mail Stop 190, Member AIAA.

†Senior Research Engineer, Structural Mechanics and Concepts Branch, MS 190, Member AIAA.

‡Senior Research Engineer, Structural Mechanics and Concepts Branch, MS 190, Associate Fellow AIAA.

§Senior Control Systems Engineer.

¶Mechatronics Engineer.

||Chief Technologist, Senior Member AIAA.

G	Gear ratio
ISS	International Space Station
$K_{Q,R}$	PID control gains, where $Q \in \{p, i, d\}$ and $R \in \{\theta, T\}$
L_i	Distance from i -th joint to link cable attachment position (m)
LSMS	Lightweight Surface Manipulation System
MDA	MacDonald, Dettwiler and Associates
M_i	Moment at the i -th joint applied by F_{tip} (Nm)
m_{tip}	Mass at the TALISMAN tip (kg)
NASA	National Aeronautics and Space Administration
J, J^{-1}	Jacobian matrix and Inverse Jacobian matrix
P_i	Global position of the i -th joint
PID	Proportional Integral Derivative control
R_C	Capstan radius (m)
s_β	Intermediate variable for inverse kinematics calculation
SRMS	Shuttle Remote Manipulator System
SSRMS	Space Station Remote Manipulator System
S_1, S_2, S_3	Intermediate variables for Inverse Jacobian calculation
TALISMAN	Tendon-Actuated Lightweight In-Space MANipulator
t	Time (s)
t_a	Time in acceleration phase in motion planning (s)
t_c	Time in coasting phase in motion planning (s)
$T_{i,c}$	Tension on the c -side of the i -th link (N)
$T_{i,MAX}$	Maximum allowable tension on joint i (N)
$T_{i,MIN}$	Minimum allowable tension on joint i (N)
$T_{i,set}$	Setpoint tension on variable tension cables, used in PID control (N)
v_i	Velocity at joint i ($\frac{m}{s}$)
\mathbf{x}	Free parameter vector $\{x, y, \theta_1\}^T$
$\{x, y\}$	Endpoint position (m)
x_t, y_t	Intermediate variables for inverse kinematics calculation
$\{X_{i,c}, Y_{i,c}\}$	Spreader cable attachment position on the c -side of the i -th link relative to the i -th joint (m)
$Z_{i,c}$	Cable length on the c -side of the i -th link, where $c \in \{a, b\}$ (m)
$\gamma_{i,c}$	Angle between i -th link and cable at the link cable attachment point (rad)
$\Delta\theta$	Change in angle for calculating planned motions (rad)
$\boldsymbol{\theta}$	Angle vector $\{\theta_1, \theta_2, \theta_3\}^T$ (rad)
$\theta_{i,C}$	Capstan angle (rad)
$\theta_{i,M}$	Motor angle (rad)
$\theta_{i,MAX}$	Maximum angle at joint i (rad)
θ_i	Angle of the i -th link relative to the $(i - 1)$ -th link (rad)
$\boldsymbol{\theta}_{set}$	Angle vector setpoint $\{\theta_{1,set}, \theta_{2,set}, \theta_{3,set}\}^T$ (rad)
$\tau_{i,M}$	Motor torque at joint i (Nm)

I. Introduction

Devices for maneuvering and precisely placing payloads are critical for efficient space operations involving reusable assets or in-space assembly and construction. Key to the success of many NASA space activities has been the availability of long-reach manipulators, such as the Shuttle Remote Manipulation System (SRMS) and the Space Station Remote Manipulation System (SSRMS). These devices have been used for many operations including berthing spacecraft, space station assembly, astronaut positioning, payload transfer, satellite deployment and spacecraft inspection prior to reentry. New missions and applications currently being considered, such as asteroid retrieval and redirection, asteroid mining, satellite servicing, and small payload delivery to future space stations or locations, can all benefit from long reach manipulators.

Current manipulators embody an architecture whereby carbon composite tubes are joined by revolute joints, with the joints accounting for the majority of the device mass. Generally, the joints are driven by a gear train that applies the joint torque relatively close to the joint axis, resulting in the need to generate large

torques, which in turn, requires large and massive gear-train-motor combinations. The area around the joint becomes a crowded location from a design stand point due to gearing, motors, and associated electronics all vying for space. Design is further complicated by the need to route a large electrical harness through the joint area to transmit power, sensor data, control and video signals between the joints and end-effector.

The current state-of-the-art in long-reach space robotics is represented by the SRMS¹ and the SSRMS² mentioned previously. Both of these incorporate the traditional manipulator architecture, consisting of lightweight booms connected by massive rotary joints that are systems of motors, gearboxes and brakes. The rotary joints account for 85 to 90 percent of the manipulator mass, as well as the manipulator compliance (in response to an applied load). The long booms severely limit the packaging options, and adding joints to improve packaging would incur an extremely high mass penalty. Thus, the high mass and compliance associated with the joints results in practical limits to: reach, packaging, stiffness, and tip force that can be achieved with the conventional robotic architecture.

In order to enable future missions and applications, it is desirable to improve space manipulator state-of-the-art by significantly increasing manipulator reach, dexterity and packaging efficiency while reducing manipulator mass and complexity. The Tendon Actuated Lightweight In-Space MANipulator (TALISMAN)^{3,4} is an innovative new robotic manipulator architecture that incorporates a tendon-actuated joint with a novel hinge that allows a full 360-degree rotation between connecting links and the capability to incorporate auxiliary and passive tension stiffening. Tendon actuation incorporates spreaders to achieve longer moment arms between the force applied by tension cables and the joint rotation axis, thus gaining mechanical advantage for generating moments and actuating the joints.

Key features of the new TALISMAN architecture and approach are:

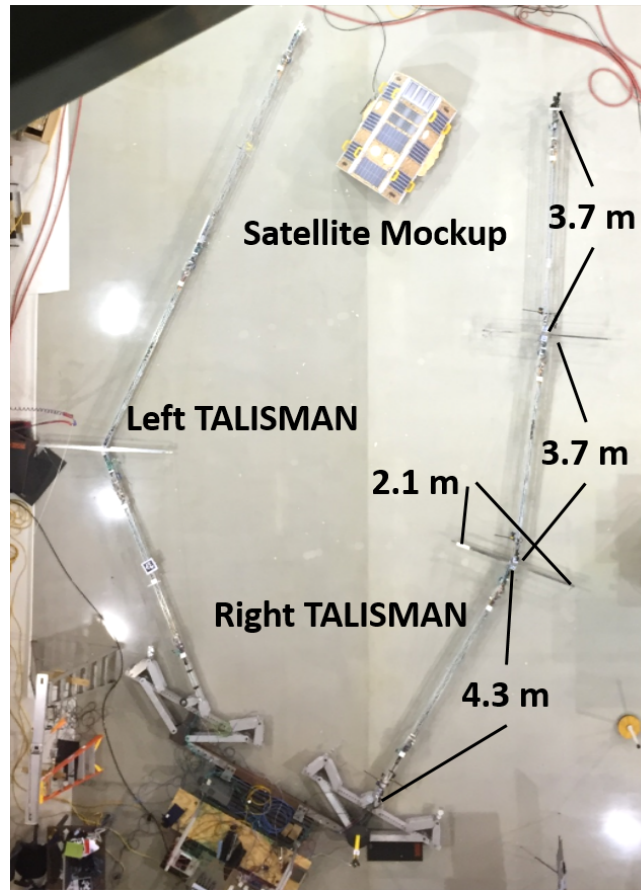
- Uses tendon actuation, which can be semi or fully antagonistic, with major components being the link, spreader, and lightweight cables, motors, and gearboxes
- Increased joint stiffness due to tendon architecture
- Lightweight joints enable the number of joints to be optimized to achieve desired packaging efficiency, range-of-motion, dexterity, etc.
- Potential to increase manipulator stiffness using passive tension elements (very lightweight)
- Versatility; many different cable/motor/control options can be implemented
- Modularity; links and joints are easy to scale for different applications, can combine link and joints as needed for packaging, dexterity, etc. to achieve operational needs
- Novel hinge joint allows full 360-degree rotation between adjacent links, improving dexterity and range of motion
- Uses lightweight truss structures for links.

The TALISMAN architecture embodies and adds to many of the features that were developed for a new planetary surface hybrid crane/manipulator, the Lightweight Surface Manipulation System (LSMS).⁵ The LSMS is a cable-actuated manipulator that achieves high structural efficiency by using a pure tension / compression structural architecture (as opposed to the beam bending architecture found in conventional robotic manipulators). Further mass efficiency is achieved by using the tension structure (cables) to also articulate the LSMS arm hinges. The tension cables provide mechanical advantage about the joint enabling small lightweight hoists or capstans to reel cable in and out (thus articulating the hinge), replacing the massive high-torque motor gear-boxes used in a conventional boom manipulator. The major distinctions between the LSMS and the TALISMAN are: the LSMS is designed to work for planetary gravity up to 1 g, the LSMS stands vertically, and has tension elements on only the top side.

A conceptual mission is shown in Figure 1(a), in which a servicing spacecraft (lower left) uses a TALISMAN to capture the Hubble Space Telescope. A laboratory demonstration of such a servicing mission is described in this paper. Currently, two TALISMAN prototypes have been assembled in the laboratory, as shown in Figure 1(b). The laboratory has a large-area flat floor that serves as an air bearing surface, and air bearings are mounted to both TALISMANs allowing zero gravity operations to be simulated in the plane of the floor. The two TALISMANs are attached to a large steel plate that represents a spacecraft bus, and the plate is also supported by air bearings allowing a spacecraft with two manipulators to be simulated



(a): Conceptual servicing mission.



(b): Above view of prototypes.

Figure 1. (a): an artist’s concept of a servicing mission employing a TALISMAN to service the Hubble Space Telescope. (b): an above view photograph of the two TALISMAN prototypes, with link and spreader lengths shown, rest on an air-bearing floor and enclose a satellite mockup for the servicing demonstration. The left TALISMAN in (b) does not have a spreader at the third joint in this photograph, making it functionally a two link TALISMAN with a double-length second link.

in experiments. Each TALISMAN has three degrees of freedom (DOF) and three links. The dual 3-link TALISMAN setup will be used extensively to develop and test operational scenarios.

In order to enable the next phase of technology development; planning and executing robotic operations, a control system has been designed and implemented on the TALISMAN. The control system is responsible for safely executing all of the tasks envisioned for the TALISMAN, and implements both joint control and endpoint control while preventing tension overload in the tendons.

The hardware implementation of the control system consists of motors (with gearboxes), tension sensors, joint angle sensors, and motor controllers, all controlled by a computer embedded at the base. The embedded computer communicates to an external control and graphical user interface (GUI) computer and to a number of actuators and sensors. Each joint is operated by two servomotors (except for the base, which only has one motor). The tension on the cables is measured using a load cell, one per joint, and the angle of each joint is measured in two ways: rotary sensors on each motor and a combination of four joint angle sensors on each joint.

The software implementation of the control system uses the external control computer for high level control, and the embedded computer software to communicate between the control computer and all of the sensors and motors on the TALISMAN. Each TALISMAN can be controlled to a specified joint angle position, joint angle velocity, endpoint Cartesian position, or endpoint Cartesian velocity. For positional control, the desired endpoint position is transformed by an inverse kinematics⁶ system of equations into a pair of joint angles, plus a free parameter for the base joint angle. For velocity control, the desired endpoint velocity is transformed by the inverse Jacobian matrix⁶ (derived from the inverse kinematic equations) into

a set of angle velocities. The base joint angle velocity is treated as a free parameter. These high level calculations of the desired motions are then converted into servomotor commands which are then input into the TALISMAN system. The tension sensors and rotary sensors are used for closed loop control, with the control performed by two proportional-integral-derivative (PID) controllers,⁷ one of which is used to control the joint pose, and one of which prevents excessive tension in the cables. To enable fine motor control and dexterity required for satellite servicing missions, a small dexterous manipulator was attached to the end of one of the TALISMANS. The dexterous manipulator is a 7-DOF manipulator with a standard pinching gripper, and an onboard high-definition camera.

The tensions, velocities, and associated equations to maneuver and capture payloads of various masses are described and discussed in this paper. Additionally, with a satellite mockup, it is possible to perform satellite servicing experiments. To demonstrate the efficacy of the TALISMANS for satellite servicing, a grasping and inspection task utilizing both TALISMANS to hold and inspect the satellite was performed, and is described in this paper. Potential improvements to the control system are then discussed.

II. Control Hardware

A single joint between two links has the following characteristics: the pretensioned cables form a quadrilateral connecting the opposite ends of the joined links to the tips of the spreader, with the tension forces balanced by compression in the links and the spreader. In an *active-active* configuration, each variable tension cable, called an *active* cable, is independently controlled by a single motor, enabling the manipulator stiffness to be varied. In the *active-passive* configuration implemented on the prototypes shown in Figure 1 and illustrated in Figure 2, two of the four cables, called *passive* cables, are attached to constant force springs, which reduce the number of motors required from four to two per joint. This configuration also reduces the number of cables requiring active tension control from four to two per joint. To reduce the cable count from four to two, capstans and pulleys allow a single cable to have variable tension on one length of cable entering the capstan and constant tension on the length of cable exiting the capstan. The capstan is a device that enables a cable wrapped around it to have different tensions as the cable enters and exits the capstan system. The active side of the cable dictates the joint shape, while the passive side balances the forces. The passive cable wraps around a pulley to provide tension to two sides of the tension quadrilateral, and connects to a constant force extensible spring embedded in the opposing link. An additional cable system, symmetric about the spreader, is also present, resulting in there being two parallel cables at the top surface, doubling the tension force provided by a single spring.

Due to the modular nature of the prototypes, it was determined that a scalable real-time control system was required. Beckhoff Automation GmbH and Co. KG⁸ was selected because they provide scalable electronics and control hardware, operated by a real-time embedded computer, which can be easily modified. Also, Beckhoff hardware is well suited to operate motors, and read from a variety of sensors, including load cells and angle encoders.^a

II.A. Power

Each TALISMAN has three power buses: a 72 V line, a 24 V line, and a 12V line (Figure 3(a)). The 72 V line is used exclusively for powering the motors, which is done by downscaling the 72 V to 24 V at each joint. The 24 V line, distinct from the 72 V downscaled voltage, powers the Beckhoff hardware. The 12 V line is used for the tension load cells.

II.B. Embedded Computer and EtherCAT Network

The embedded computer that operates both TALISMAN prototypes is a Beckhoff CX5020 (Figure 3(a)). This computer, located at the base of the prototypes, uses an Intel Atom Z530 processor, which operates at 1.6 GHz. Its main memory is a 128 megabyte compact flash memory card, on which is installed the Windows Embedded Standard 2009 real-time operating system. The CX5020 communicates with all of the Beckhoff hardware embedded on the arms using the EtherCAT standard, a protocol designed by Beckhoff that is suitable for real-time requirements. In addition to sending commands and reading sensor inputs at fixed intervals, the CX5020 operates control software using two layers: a TwinCAT layer for communicating

^aReference to any specific commercial products, process, or service by trade name, trademark, manufacturer, or otherwise, does not constitute or imply an endorsement, recommendation, or preference by NASA.

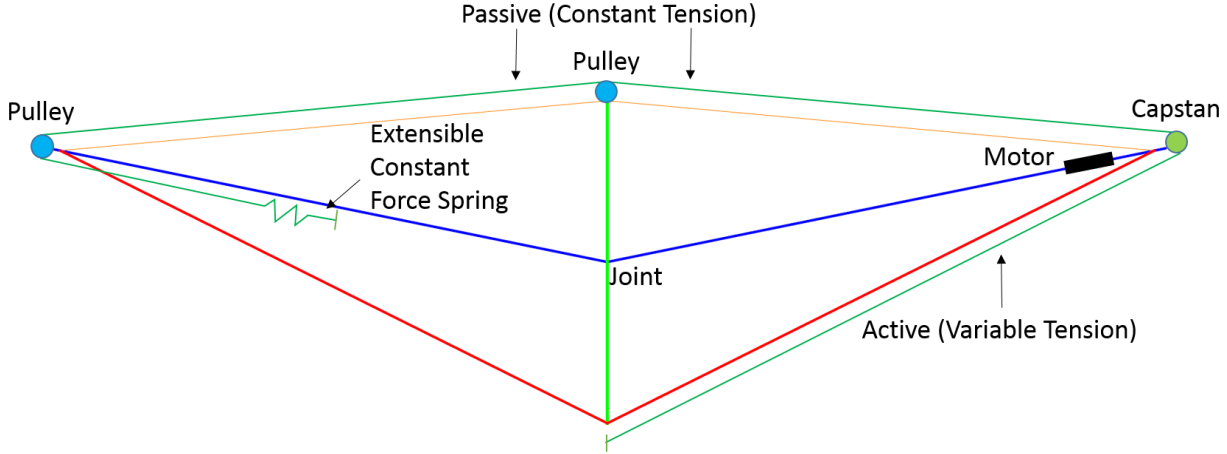


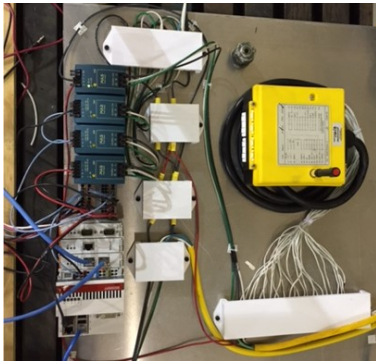
Figure 2. The layout of a single cable on the TALISMAN. The TALISMAN prototypes use *active-passive* tensioning to achieve their pose, using only two cables and two motors. The other cable (not shown) is a reflection over the spreader axis.

the real-time inputs and outputs to an external computer, and a compiled Simulink layer for implementing the control system. The TwinCAT layer uses the Structured Text programming language to communicate between the Simulink application and the actuators and sensors. The CX5020 communicates to the Beckhoff hardware at a frequency of 200 Hz, and executes an instance of the Simulink application at a frequency of 500 Hz. Additionally, the CX5020 maintains an Ethernet connection to an external computer, which operates TwinCAT software, and enables a user to issue commands to the TALISMANS.

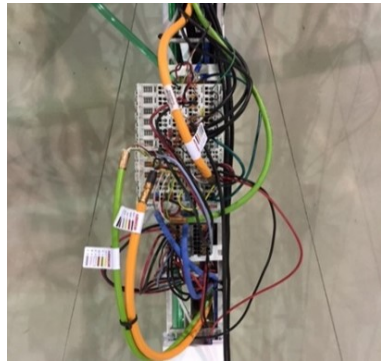
The EtherCAT network on which the CX5020 is the root is a two-branch tree; the base joints of each prototype are the child nodes of the root, the second joints are the child nodes of the base joints, and the third joints are the child nodes of the second joints. Communications from the third joint, for example, are passed through the second and base joints to the CX5020. At each joint are a number of terminal nodes, which are directly responsible for the actuators and the sensors. The branching node is the EK1122, which joins the EtherCAT cables from both arms and prevents one arm from being a child to the other arm. At each joint is an EK1100 node, which serves two purposes: to connect the terminal nodes to the network, and to enable additional EK1100 nodes further down the connectivity chain to communicate to the CX5020. A single terminal cluster is shown in Figure 3(b).

II.C. Joint Motors

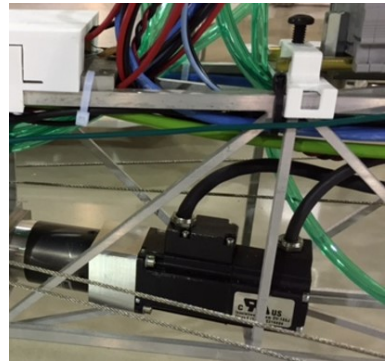
Each TALISMAN prototype makes use of just one kind of motor, each of which is connected by a gearbox to a capstan. The active portion of the cable attaches to the tip of the spreader, enters and wraps once around the capstan, exits the capstan, and connects to an extendable constant force spring after passing over a pulley at the spreader tip and a pulley at the end of the opposing link. Friction between the cable and the capstan enables the difference in tensions on the portions of cable entering and exiting the capstan; the friction can be increased by increasing the number of wraps. The geometry of the spreader and the link is determined by the tension and the length of the active cable, which is changed by rotating the capstan. To drive the capstans, the Beckhoff AM3111 synchronous servomotor was chosen (Figure 3(c)), paired with an EL7201 servomotor terminal. The servomotor has a rated torque is 0.16 Nm, a rated speed of 3000 revolutions per minute, and requires 50 W at 24 V, with a constant current of 3.22 A when standing current, and a peak current of 10.6 A when actuating. The torque constant is $0.5 \frac{\text{Nm}}{\text{A}}$, and the voltage constant is 3.0 mV revolutions per minute. Each motor also includes a resolver, which provides angular position data to the EL7201, which is then transmitted to the CX5020. The servomotor drives the capstan through two gearboxes, enabling a larger torque: a Beckhoff-designed 64:1 gearbox, paired with a 5:1 TALISMAN gearbox (Figure 3(d)), provides a gear ratio $G = 320$ rotations of the motor for 1 rotation of the capstan, increasing the rated torque to 51.2 Nm.



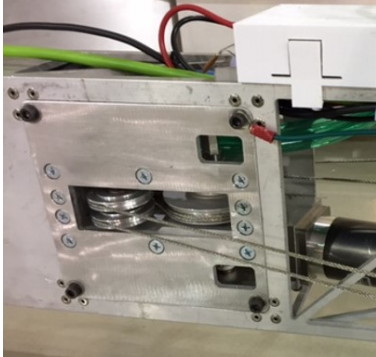
(a): Power and CX5020 computer.



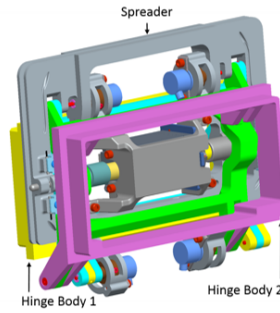
(b): Joint terminal.



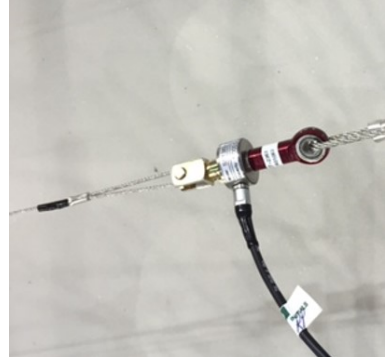
(c): AM3111 motor.



(d): Capstan and pulleys.



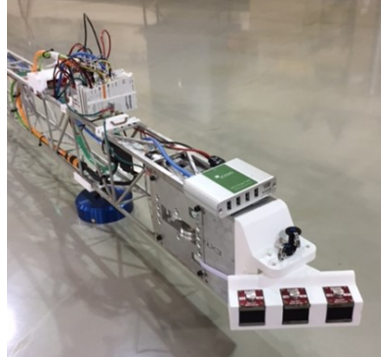
(e): Hinge bodies and spreader.



(f): Toledo tension load cell.



(g): Robai Cyton Gamma 1500



(h): Magnetic end-effector.



(i): Ametek constant force spring.

Figure 3. Various control components used on the TALISMAN prototypes, including the joints.

II.D. Angle Encoders

Each joint, with the exception of the base joint, consists of the two adjacent links, the spreader, and a hinge system (which enables the two links to be folded at $\pm 180^\circ$ from the fully extended position, and achieves the full 360-degree range of the joint⁹) as shown in Figure 3(e). To characterize the joint state, four angle measurements are required (only one is needed for the base joint). These are the angles between:

- Link 1 and hinge body 1
- Hinge body 1 and the spreader
- Hinge body 2 and the spreader
- Link 2 and hinge body 2.

The Contelec Vert-X 13E,¹⁰ an analog magnetic contact-free angle sensor, was selected to measure these angles. It provides analog measurements through its full 360-degree range as a voltage scaled between 10% and 90% of 10 V. The Beckhoff EL3164 10 V analog input terminal converts the analog signal to a 16 bit digital signal, which is then transmitted to the CX5020.

II.E. Load Cells

One of the two active cables controlling each joint is equipped with a load cell which measures the tension in the cable. Due to symmetry, the other active cable is assumed to have the same tension. The load cells, provided by Toledo Transducers, Inc.¹¹ (Figure 3(f)), are rated at 1000 lb, and are connected to the 12 V power supply. Each cell is connected to a Beckhoff EL3356-0010 resistor bridge, which converts the load cell signal into a digital value, and transmits this value to the CX5020.

II.F. End-Effectors

Each TALISMAN prototype is outfitted with a different end-effector. The right prototype is equipped with a Robai Cyton Gamma 1500¹² robotic manipulator (Figure 3(g)). The Cyton is a 7-DOF robotic manipulator with a high definition camera (Figure 3(g)) and a two-prong gripper. As a 7-DOF arm, it is kinematically redundant, enabling a continuum of possible poses to place the gripper at a certain position and orientation. The arm is connected to the 12 V power supply, and communicates to the teleoperation computer via Universal Serial Bus, making it separate from the Beckhoff system. While the gripper enables pick-and-place tasks and bolting/unbolting, for the demonstration in this paper, the Cyton was used only as a mobile camera for satellite inspection.

The left prototype is equipped with a passive magnetic gripper end-effector (Figure 3(h)). This gripper pivots about an axis normal to the TALISMAN plane of motion, and enables passive joining to any magnetic object. The satellite mockup is equipped with a steel plate, and can self-attach to the gripper provided the distance and velocity normal to the gripper are small.

II.G. Constant Force Springs

The constant force springs used by the TALISMAN arms (Figure 3(i)) are Ametek Negator B Motor ML-2482¹³ model springs. They provide 66.7 N of constant tension, and can extend up to 4.064 m.

III. Control

The Beckhoff CX5020 executes a compiled Simulink program at a frequency of 500 Hz. This program, designed by MacDonald, Dettwiler and Associates (MDA) US Systems, implements a quasi-static motion controller, with the following assumptions and simplifications:

- Each joint is modeled as a single hinge joint, eliminating the intermediate hinge bodies and fixing the rotation axis relative to the links.
- Each spreader bisects the angle between the links, which requires calibration on the prototypes.
- The lever arms of the cables on each end of each spreader have equal length, making the tension vectors symmetric about the spreader axis.
- All motion is quasi-static, so structural dynamics can be ignored.

These simplifications enable an inverse kinematics and inverse Jacobian formulation to be used that are easily described and quickly calculated for transforming desired joint and endpoint velocities to cable actuation velocities. Two PID controllers, one to close on the desired position and one to prevent excessive tension, operate in parallel and are summed to produce a single output.

With the aforementioned assumptions, the TALISMAN prototypes are both 3-DOF manipulators, with link lengths d_1 , d_2 , and d_3 and link angles θ_1 , θ_2 , and θ_3 as shown in Figure 4. The active cables are shown in red, the passive cables are shown in orange, the links are shown in blue, and the spreaders are shown in green. Each joint is labeled from 1 to 3, and each cable labeled: a, a', b, and b'.

Due to symmetry, any cable with a prime will share the same characteristics as the cable without a prime; thus, for the remainder of the paper, only cables without a prime will be described.

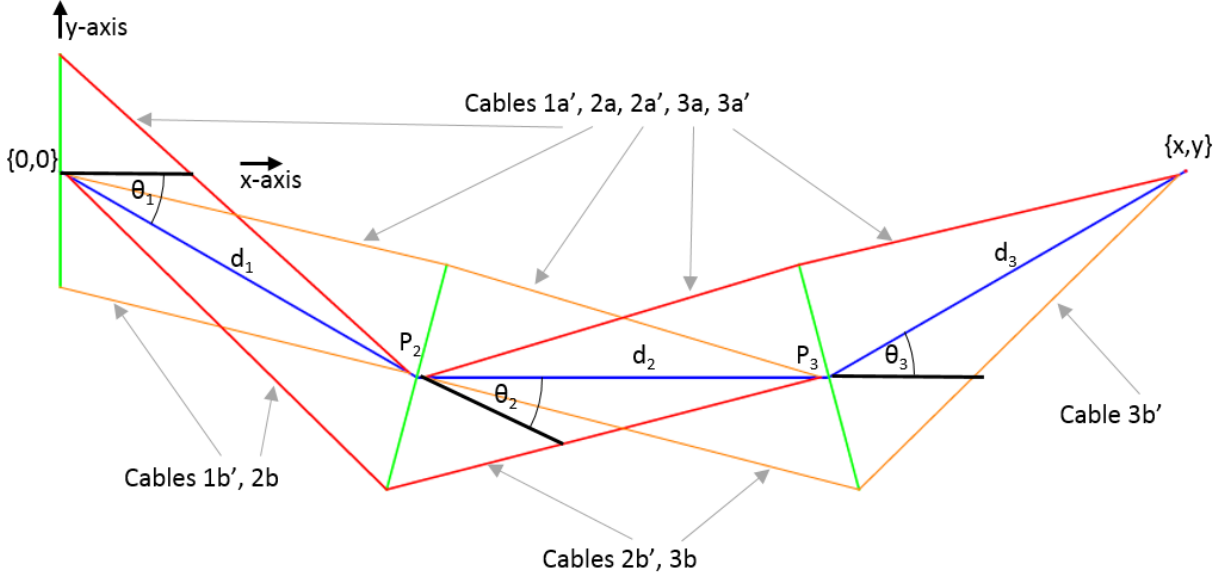


Figure 4. Diagram of a TALISMAN prototype. The three links, with lengths d_1, d_2 , and d_3 , are shown in blue. The angles, θ_1, θ_2 , and θ_3 , are relative to the previous link, with the angle of the base link being relative to the origin. The cables are identified, with “a” referring to the positive-y side, and prime (') referring to the distal side, of each joint. The green lines are the spreaders, the red lines are the active cables in the *active-passive* antagonistic system, and the orange lines are the passive cables in the same system.

III.A. Forward and Inverse Kinematics

The Cartesian position of the endpoint, $\{x, y\}$, as a function of the three angles, is given in Equation 1, and defines the forward kinematics of the TALISMAN. To simplify the calculations in the following sections, the base joint angle, θ_1 , is considered a free parameter, and is included in the full position vector \mathbf{x} .

$$\mathbf{x} = \begin{pmatrix} x \\ y \\ \theta_1 \end{pmatrix} = \begin{pmatrix} \cos(\theta_1) d_1 + \cos(\theta_1 + \theta_2) d_2 + \cos(\theta_1 + \theta_2 + \theta_3) d_3 \\ \sin(\theta_1) d_1 + \sin(\theta_1 + \theta_2) d_2 + \sin(\theta_1 + \theta_2 + \theta_3) d_3 \\ \theta_1 \end{pmatrix} \quad (1)$$

The inverse kinematics of the TALISMAN can be found by calculating the angles θ_1, θ_2 , and θ_3 as a function of $\{x, y\}$. Since the number of angles is greater than the endpoint position dimensions, there is a one-dimensional continuum of possible angle combinations that result in the correct endpoint. One method of reducing the dimensionality is choosing one of the parameters to be fixed, for example θ_1 . Then, assuming the distance between the end of the first link and the endpoint is less than or equal to the total length of the remaining links, there are two solutions, each one a reflection of the other about the line between the first link tip and the endpoint. The steps required to calculate the remaining angles, θ_1 and θ_2 , are given in Equations 2 to 10, and use intermediate variables $x_t, y_t, c_3, d_t, c_\beta$, and s_β to simplify the expression. Equation 6 returns the two possible angles that satisfy the relationship; the remaining parameters will depend on which solution to Equation 6 is used.

$$x_t = x - d_1 \cos(\theta_1) \quad (2)$$

$$y_t = y - d_1 \sin(\theta_1) \quad (3)$$

$$c_3 = \frac{-d_2^2 - d_3^2 + x_t^2 + y_t^2}{2d_2d_3} \quad (4)$$

$$d_t = \frac{1}{x_t^2 + y_t^2} \quad (5)$$

$$\theta_3 = \pm \tan^{-1} \left(c_3, \sqrt{1 - c_3^2} \right) \quad (6)$$

$$c_\beta = d_t ((c_3 d_3 + d_2) x_t + d_3 y_t \sin(\theta_3)) \quad (7)$$

$$s_\beta = d_t ((c_3 d_3 + d_2) y_t - d_3 x_t \sin(\theta_3)) \quad (8)$$

$$\theta_2 = \tan^{-1}(c_\beta, s_\beta) - \theta_1 \quad (9)$$

$$\boldsymbol{\theta} = \begin{pmatrix} \theta_1 \\ \theta_2 \\ \theta_3 \end{pmatrix} \quad (10)$$

To reduce the likelihood of arm self-collision, the algorithm chooses the θ_3 that minimizes θ_2 . If the total length of the final two links is less than the distance between the first link and the endpoint, θ_3 is set to zero, and θ_2 is set to point the two links along the vector to the endpoint.

III.B. Endpoint Velocity to Joint Angular Velocity

In addition to calculating the angles required to position the endpoint, it is desirable to calculate the angular velocities required to move the endpoint at a desired rate. With the forward and inverse kinematics relations established in Equations 1, 6, and 9, the angular velocity required to match a desired endpoint velocity can be derived. Let the endpoint velocity be $\frac{d\mathbf{x}}{dt}$. Following the chain rule, the angular velocities at the joints required to drive the endpoint at the desired velocity are:

$$\frac{d\boldsymbol{\theta}}{dt} = \frac{d\boldsymbol{\theta}}{d\mathbf{x}} \frac{d\mathbf{x}}{dt} = \left(\frac{d\mathbf{x}}{d\boldsymbol{\theta}} \right)^{-1} \frac{d\mathbf{x}}{dt} = J^{-1} \frac{d\mathbf{x}}{dt} \quad (11)$$

The Jacobian matrix, J , is the rate of change of the forward kinematics expressions with respect to the angles. Following the inverse function theorem, the inverse Jacobian matrix J^{-1} is the Jacobian of the inverse kinematics expression, and is calculated in Equations 12 to 18, using intermediate variables C_1, C_2, C_3, S_1, S_2 , and S_3 :

$$C_1 = d_1 \cos(\theta_1) \quad (12)$$

$$C_2 = d_2 \cos(\theta_1 + \theta_2) \quad (13)$$

$$C_3 = d_3 \cos(\theta_1 + \theta_2 + \theta_3) \quad (14)$$

$$S_1 = d_1 \sin(\theta_1) \quad (15)$$

$$S_2 = d_2 \sin(\theta_1 + \theta_2) \quad (16)$$

$$S_3 = d_3 \sin(\theta_1 + \theta_2 + \theta_3) \quad (17)$$

$$J^{-1} = \begin{pmatrix} \frac{\partial \theta_1}{\partial x} & \frac{\partial \theta_1}{\partial y} & \frac{\partial \theta_1}{\partial \theta_1} \\ \frac{\partial \theta_2}{\partial x} & \frac{\partial \theta_2}{\partial y} & \frac{\partial \theta_2}{\partial \theta_1} \\ \frac{\partial \theta_3}{\partial x} & \frac{\partial \theta_3}{\partial y} & \frac{\partial \theta_3}{\partial \theta_1} \end{pmatrix} = \begin{pmatrix} 0 & 0 & 1 \\ \frac{\csc(\theta_3) C_3}{d_2 d_3} & \frac{\csc(\theta_3) S_3}{d_2 d_3} & \frac{\csc(\theta_3) (C_3 (S_1 + S_2) - (C_1 + C_2) S_3)}{d_2 d_3} \\ \frac{\csc(\theta_3) (-C_2 - C_3)}{d_2 d_3} & \frac{\csc(\theta_3) (-S_2 - S_3)}{d_2 d_3} & \frac{\csc(\theta_3) (C_1 (S_2 + S_3) - (C_2 + C_3) S_1)}{d_2 d_3} \end{pmatrix} \quad (18)$$

III.C. Joint Angular Velocity to Capstan Motor Velocity

To find the motor velocities required to drive the endpoint at a desired velocity, the angular velocity expression in Equation 11 must first be converted to a cable length change rate, then to a capstan revolution rate, followed by the motor rotation rate. For a single joint, the calculations can be simplified by changing the frame of reference so that a joint is at the origin, and the spreader lies along the y-axis (see Figure 5). In this frame of reference, each link deviates from the x-axis at the half angle $\frac{\theta_i}{2}$. Let L_i be the distance between the joint and the cable attachment point on each link (for each joint, this length is the same on both sides to simplify tension calculations), and the attachment points on the spreaders are $\{x_{i,a}, y_{i,a}\}$ and $\{x_{i,b}, y_{i,b}\}$. Let c be a substitute for either a or b . The length of the cable, $Z_{i,c}$ is:

$$Z_{i,c} = \sqrt{\left(L_i \cos\left(\frac{\theta_i}{2}\right) - X_{i,c} \right)^2 + \left(L_i \sin\left(\frac{\theta_i}{2}\right) - Y_{i,c} \right)^2} \quad (19)$$

Finding the derivative of $Z_{i,c}$ with respect to the angle θ_i :

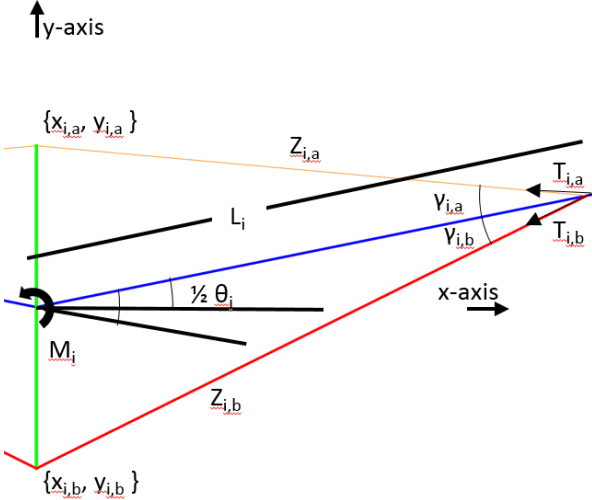


Figure 5. A joint can be plotted with the spreader overlaying the y-axis, with the joint at the origin, and each link deviating from the y-axis at angles of $\frac{\theta_i}{2}$ and $\pi - \frac{\theta_i}{2}$. This simplifies calculations of joint cable lengths and tensions. The geometry enables all values to be symmetric, with the tensions $T_{i,a}$ and $T_{i,b}$ being equal on both sides of the spreader.

$$\frac{\partial Z_{i,c}}{\partial \theta_i} = \frac{L_i (X_{i,c} \sin(\frac{\theta_i}{2}) - Y_{i,c} \cos(\frac{\theta_i}{2}))}{2\sqrt{(X_{i,c} - L_i \cos(\frac{\theta_i}{2}))^2 + (Y_{i,c} - L_i \sin(\frac{\theta_i}{2}))^2}} \quad (20)$$

Using the chain rule, the cable length change rate with respect to time is:

$$\frac{dZ_{i,c}}{dt} = \frac{\partial Z_{i,c}}{\partial \theta_i} \frac{d\theta_i}{dt} \quad (21)$$

Let the capstan radius be R_C and the capstan angle be θ_C . The angular velocity of the capstan can be calculated:

$$\frac{d\theta_{i,C}}{dt} = \frac{1}{R_C} \frac{dZ_{i,c}}{dt} \quad (22)$$

Finally, the motor rotation speed can be calculated in radians per second, in proportion to the capstan angular velocity, with gear ratio G :

$$\frac{d\theta_{i,M}}{dt} = G \frac{d\theta_{i,C}}{dt} \quad (23)$$

Equations 20 through 23, when combined with Equation 11, give the speed required for each motor to move the TALISMAN endpoint at a desired velocity. These expressions are valid for both the *active-active* and *active-passive* systems, but the latter comes with a caveat; since a capstan takes in as much cable on one side as the capstan lets out on the other, and in the general case $\frac{dZ_{i,a}}{dt} \neq -\frac{dZ_{i,b}}{dt}$, the passive cable is attached to a constant force spring that allows additional extension or retraction of the cable.

III.D. Tensions Required to Maintain Static Pose, With or Without External Loading

The frame of reference in Figure 5 also allows simple calculation of the tensions needed to maintain the pose of each joint. In the general case for a moment M_i about the joint, the tensions in the cable must balance out the moment. With the convention that the torque vectors for M_i and tension $T_{i,a}$ point in the opposite direction of tension $T_{i,b}$, the expression for cable tension is:

$$\gamma_{i,c} = \arccos \left(\frac{L_i^2 + Z_{i,c}^2 - (X_{i,c}^2 + Y_{i,c}^2)}{2L_i Z_{i,c}} \right) \quad (24)$$

$$L_i T_{i,b} \sin(\gamma_{i,b}) = L_i T_{i,a} \sin(\gamma_{i,a}) + M_i \quad (25)$$

The angles $\gamma_{i,a}$ and $\gamma_{i,b}$ represent the angle at which the tension acts. The smaller the angle, the smaller the lever arm, and the larger the tension must be; longer spreaders enable greater induced moments on the joints.

If a force F_{tip} is acting on the tip (see Figure 6), each joint at position P_i will experience a moment equal to:

$$M_i = (\{x, y\} - P_i) \times F_{tip} \quad (26)$$

Equations 25 and 26 enable the calculation of all tensions required to maintain the pose under an arbitrary tip load. As the distance from the tip to any joint increases, the moment at the joint increases, leading to the base joint being subject to the largest moments.

III.E. Tensions Required to Accelerate a Mass at the Endpoint

An inertial mass attached to the endpoint of the TALISMAN will resist a change in velocity; this reaction force can be modeled as a tip force, F_{tip} . Since the TALISMAN is expected to be far less massive than the payload, the reaction force from the TALISMAN itself will contribute little to the calculation, and can be ignored for quasi-static motions^b. Additionally, this model assumes a fixed base, an assumption that is valid if the spacecraft on which the TALISMAN is mounted has a mass much larger than both the TALISMAN and objects held at the tip. This assumption holds for all subsequent analyses in this paper.

The velocity and acceleration at the tip given angular velocities and angular accelerations can be calculated using standard rigid body expressions,¹⁴ resulting in the following equations:

$$v_1 = \frac{d\theta_1}{dt} \times P_1 \quad (27)$$

$$v_2 = v_1 + \left(\frac{d\theta_1}{dt} + \frac{d\theta_2}{dt} \right) \times (P_2 - P_1) \quad (28)$$

$$v_3 = v_2 + \left(\frac{d\theta_1}{dt} + \frac{d\theta_2}{dt} + \frac{d\theta_3}{dt} \right) \times (P_3 - P_2) \quad (29)$$

$$a_1 = \frac{d\theta_1}{dt} \times \left(\frac{d\theta_1}{dt} \times P_1 \right) + \frac{d^2\theta_1}{dt^2} \times P_1 \quad (30)$$

$$a_2 = a_1 + \left(\frac{d\theta_1}{dt} + \frac{d\theta_2}{dt} \right) \times \left(\left(\frac{d\theta_1}{dt} + \frac{d\theta_2}{dt} \right) \times (P_2 - P_1) \right) + \left(\frac{d^2\theta_1}{dt^2} + \frac{d^2\theta_2}{dt^2} \right) \times (P_2 - P_1) \quad (31)$$

$$a_3 = a_2 + \left(\frac{d\theta_1}{dt} + \frac{d\theta_2}{dt} + \frac{d\theta_3}{dt} \right) \times \left(\left(\frac{d\theta_1}{dt} + \frac{d\theta_2}{dt} + \frac{d\theta_3}{dt} \right) \times (P_3 - P_2) \right) + \left(\frac{d^2\theta_1}{dt^2} + \frac{d^2\theta_2}{dt^2} + \frac{d^2\theta_3}{dt^2} \right) \times (P_3 - P_2) \quad (32)$$

The true angular velocities and accelerations of each link in the fixed frame of reference are the sums of all of the first and second derivatives of each link prior to the reference link with each θ_i being measured with respect to the previous link.

The instantaneous acceleration of the payload mass m_p (with the assumption that the mass is concentrated at the tip) is a_3 . The reactive force on the tip of the TALISMAN points in the opposite direction of a_3 , and can be calculated as:

$$F_{tip} = -m_p a_3 \quad (33)$$

^bThe individual force contributions from each body in the TALISMAN, in general, cannot be ignored in a dynamic system, and will contribute to the calculation of the vibration modes.

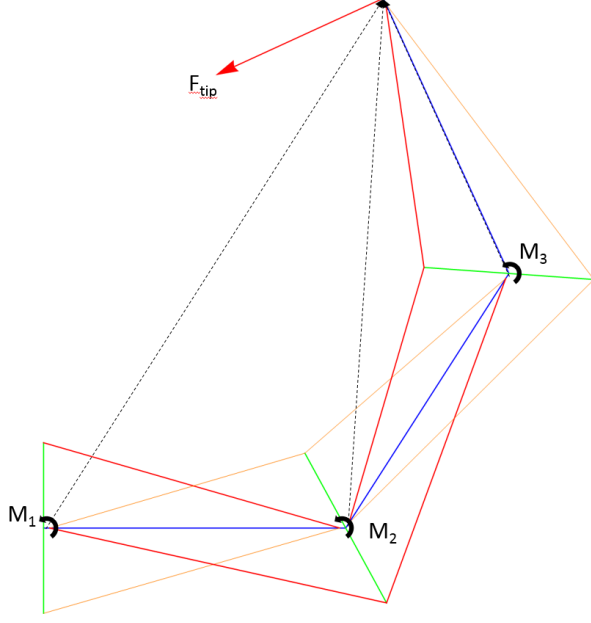


Figure 6. The moments induced at each joint due to a tip force F_{tip} are found by calculating the cross product of the vector from the joint to the tip (black dotted lines) with the force vector, as shown in Equation 26.

Equation 33 can be combined with Equations 25 and 26 to calculate the instantaneous moments at each joint, and the tensions required in the cables.

III.F. Motion Planning

Four different methods for controlling the TALISMAN prototypes have been implemented:

- Command to joint velocity
- Command to endpoint velocity
- Command to joint position
- Command to endpoint position.

When commanding the joint or endpoint velocity directly, the controller will linearly ramp the angle velocities from zero to the set velocity at an acceleration no greater than $\frac{d^2\theta_{i,MAX}}{dt^2} \frac{\text{rad}}{\text{s}^2}$. When commanding to a specified joint or endpoint position, the angular velocity follows a calculated trapezoidal profile, ramping up at the start and slowing down when approaching the goal, as shown in Figure 7. When the angle change for each joint is not the same, the acceleration and constant angular velocity phases for each joint are scaled so that they complete the move at the same time. For a desired coasting fraction of f_c , maximum angular acceleration of $\frac{d^2\theta_{i,MAX}}{dt^2}$, the acceleration/deceleration time t_a and coasting time t_c can be found for any angle change Δ_θ :

$$\Delta_\theta = \theta_{set} - \theta(0) \quad (34)$$

$$\beta = \frac{2f_c}{1 - f_c} \quad (35)$$

$$t_a = \max \sqrt{\frac{\|\Delta_\theta\|}{(1 + \beta) \frac{d^2\theta_{i,MAX}}{dt^2}}} \quad (36)$$

$$t_c = \beta t_a \quad (37)$$

$$(38)$$

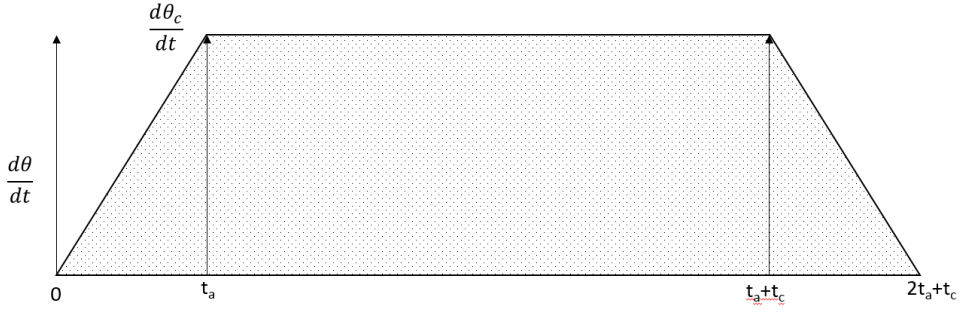


Figure 7. The velocity profile for an angle change $\Delta\theta$.

The angular acceleration, $\frac{d^2\theta_a}{dt^2}$, can then be calculated, as well as the angular velocities, $\frac{d\theta}{dt}(t)$, and angles, $\theta(t)$, at time t :

$$\frac{d^2\theta_a}{dt^2} = \begin{cases} \frac{\Delta\theta}{t_a(t_a+t_c)} & \text{if } t \leq t_a \\ 0 & \text{if } t_a < t \leq t_a + t_c \\ -\frac{\Delta\theta}{t_a(t_a+t_c)} & \text{if } t_a + t_c < t \leq 2t_a + t_b \end{cases} \quad (39)$$

$$\frac{d\theta}{dt}(t) = \begin{cases} \frac{d^2\theta_a}{dt^2}t & \text{if } t \leq t_a \\ \frac{d^2\theta_a}{dt^2}t_a = \frac{d\theta_c}{dt} & \text{if } t_a < t \leq t_a + t_c \\ \frac{d^2\theta_a}{dt^2}t_a - \frac{d^2\theta_a}{dt^2}(t - t_a - t_c) & \text{if } t_a + t_c < t \leq 2t_a + t_b \end{cases} \quad (40)$$

$$\theta(t) = \begin{cases} \frac{d^2\theta_a}{2dt^2}t^2 & \text{if } t \leq t_a \\ \frac{d^2\theta_a}{2dt^2}t_a^2 + \frac{d\theta_c}{dt}(t - t_a) & \text{if } t_a < t \leq t_a + t_c \\ \frac{d^2\theta_a}{2dt^2}t_a^2 + \frac{d\theta_c}{dt}t_c + \frac{d\theta_c}{dt}(t - t_a - t_c) - \frac{d^2\theta_a}{2dt^2}(t - t_a - t_c)^2 & \text{if } t_a + t_c < t \leq 2t_a + t_b \end{cases} \quad (41)$$

III.G. PID Control

Two PID controllers are summed to provide additional velocity to the motors; one to approach the desired position and one to approach the desired tension. The PID controller supplements the control methods described in Section III.F to ensure the measured angles and tensions are near the desired angles and tensions at any time, t . For example, at time t , the measured angle may be less than the intended angle in Equation 41, which will result in an increase in angular velocity. Multiplying the error, integral of the error, and the derivative of the error by tunable gains, K , results in:

$$e_{\theta_i}(t) = \theta_{i,set} - \theta_i \quad (42)$$

$$e_{T_i}(t) = T_{i,set} - T_i(t) \quad (43)$$

$$\frac{d\theta_{i,M}}{dt} = K_{p,\theta}e_{\theta_i}(t) + K_{i,\theta}\int_0^t e_{\theta_i}(t)dt + K_{d,\theta}\frac{e_{\theta_i}(t)}{dt} + K_{p,T}e_{T_i}(t) + K_{i,T}\int_0^t e_{T_i}(t)dt + K_{d,T}\frac{e_{T_i}(t)}{dt} \quad (44)$$

Deriving the optimal choice of gains is outside the scope of this paper; only the angle proportional gain, $K_{p,\theta}$, was set to 1, while all other gains were set to 0. In the cases where the endpoint velocity or angle velocity are set *a priori*, the angle component of the PID controller is skipped, allowing direct control when all gains are equal to zero.

IV. Prototype Control Capabilities and Limitations

This section discusses the capabilities and limitations in planning and executing various maneuvers with the TALISMAN prototype. These capabilities and limitations assume a best-case control scenario in which measurements are accurate, the input delay is negligible, and the electronics and mechanics are functional and perfectly modeled, making the PID controller unnecessary.

IV.A. Parameters and Limits

The TALISMAN prototypes have the following parameters:

$$R_C = 0.0308 \text{ m} \quad (45)$$

$$G = 320 \quad (46)$$

$$d_1 = 4.3434 \text{ m} \quad (47)$$

$$d_2 = d_3 = 3.7338 \text{ m} \quad (48)$$

$$X_{i,c} = 0 \text{ m} \quad (49)$$

$$Y_{1,a} = 1.05728 \text{ m} \quad (50)$$

$$Y_{2,a} = Y_{3,a} = 1.05261 \text{ m} \quad (51)$$

$$Y_{1,b} = -1.05728 \text{ m} \quad (52)$$

$$Y_{2,b} = Y_{3,b} = -1.05261 \text{ m} \quad (53)$$

$$L_1 = 4.27 \text{ m} \quad (54)$$

$$L_2 = L_3 = 3.66 \text{ m} \quad (55)$$

$$T_{1,b} = T_{2,a} = T_{3,c} = 30 \text{ lb} = 133.45 \text{ N} \quad (56)$$

The TALISMAN is designed to manipulate objects far more massive than the TALISMAN itself, so two target masses, representing a low mass and high mass satellite, were selected for determining the capabilities of the TALISMAN prototypes:

$$m_{tip} \in \{200, 3000\} \text{ kg} \quad (57)$$

The capabilities and limitations must obey the following hard limits:

$$T_{i,MIN} = 5 \text{ lb} = 22.24 \text{ N} \quad (58)$$

$$T_{i,MAX} = 75 \text{ lb} = 333.62 \text{ N} \quad (59)$$

$$\pm \frac{d\theta_{i,M,MAX}}{dt} = \pm 3000 \frac{\text{rev}}{\text{min}} = \pm 100\pi \frac{\text{rad}}{\text{s}} \quad (60)$$

$$\pm\theta_{1,MAX} = \pm \frac{65\pi}{180} \text{ rad} \quad (61)$$

$$\pm\theta_{2,MAX} = \pm\theta_{3,MAX} = \pm \frac{130\pi}{180} \text{ rad} \quad (62)$$

The steel cables on the prototypes have a diameter of 0.0625 in, with an ultimate load of approximately 375 lb; with a safety factor of 5, the maximum allowable tension value is 75 lb. This not only protects against a cable failure in ultimate load, but also prevents backlash incidents and meets safety requirements for operating around humans.

IV.B. Maximum Angular Velocity

The maximum motor velocity scales to a maximum cable length change according to Equation 23:

$$\pm \frac{dZ_{i,c,MAX}}{dt} = \pm 0.0302 \frac{\text{m}}{\text{s}} \quad (63)$$

Using this with Equation 21, the maximum joint angular velocity can be found as a function of joint angle. The maximum angular velocity when extending the active cables (for joints 1 and 3, extending the active cables results in a decrease in joint angle) is shown in Figure 8; for retracting the active cables, each angular velocity maximum curve changes sign. These results can be used to set a global maximum angular velocity limit based on the absolute minimum of each curve:

$$\frac{d\theta_{1,MAX}}{dt} = \pm 0.029 \frac{\text{rad}}{\text{s}} \quad (64)$$

$$\frac{d\theta_{2,MAX}}{dt} = \pm 0.057 \frac{\text{rad}}{\text{s}} \quad (65)$$

$$\frac{d\theta_{3,MAX}}{dt} = \pm 0.057 \frac{\text{rad}}{\text{s}} \quad (66)$$

$$(67)$$

IV.C. Maximum Tension for Joint Motor Torque

In order to retract a cable under tension, the joint motor must apply a torque that pulls against the tension. Because the motor cannot be backdriven through the gearbox, this does not apply for static loads or extending the cable. The relationship between motor torque $\tau_{i,M}$ and force applied at the capstan to the cable is:

$$\tau_{i,M} = \frac{R_c T_{i,c}}{G} \quad (68)$$

The rated torque of the Beckhoff AM3111 motors is 0.16 Nm, making the maximum force applied at the capstan surface 1663 N, greatly exceeding the maximum allowable tension in the cables.

IV.D. Maneuvering Objects

This section describes the velocities, accelerations, and forces necessary to move a massive object at rest in one location to another location at rest. The full maneuver must be planned and executed without exceeding the tension and motor velocity limits. One example of such a maneuver may be to bring the grasped object closer to the base of the arm, so that another TALISMAN prototype can inspect the object. Since the TALISMAN is versatile, a wide range of possible masses should be considered, with 200 kg and 3000 kg being used in the current analyses. Differences in tip mass, starting position, and ending position will result in one of the motor velocity or cable tension limits being the driving factor. The cases presented here are feasible solutions to the constraint satisfaction problem, and do not seek to minimize a metric.

The cases examined here start with a known $\boldsymbol{\theta}(0) = \{0, 0, 0\}$ rad $\rightarrow \{x, y\}(0) = \{11.811, 0\}$ m and move to an endpoint position $\{x, y\}(t) = \{3, 1\}$ m and $\theta_1 = -\frac{\pi}{3}$ rad, which, when using the inverse kinematics in Equation 10, is $\boldsymbol{\theta}(t) = \{-\frac{\pi}{3}, 1.58, 1.73\}$ rad. The motion is planned using the trapezoid velocity profile described in Equations 39 to 41. The motors are assumed to accelerate from one velocity to another in a short time span, leading to apparently sudden jumps in tension in the time span of the maneuver.

The motion planning for a 200 kg tip mass, shown in Figure 9, is found by varying the constant angular velocity fraction f_c and the maximum angular acceleration $\frac{d^2\theta_{i,MAX}}{dt^2}$ until finding a constraint-satisfying solution, with $f_c = 0.7$ and $\frac{d^2\theta_{i,MAX}}{dt^2} = 0.008 \frac{\text{rad}}{\text{s}^2}$, requiring 41.2 s to complete. The ending position of the arm is shown in Figure 9(a). The curved line is the path taken by the endpoint, and the red lines show the directions and relative magnitudes of the reaction tip force induced by the the mass. The distinct segments include the angular acceleration and coasting phases. Figure 9(b) shows the tensions required in the cables to follow the profile, figure 9(c) shows the motor speeds, figure 9(d) shows the angular velocity trapezoids, and figure 9(e) shows the tip speed components, where the total tip speed is $\sqrt{\frac{dx^2}{dt} + \frac{dy^2}{dt}} \frac{\text{m}}{\text{s}}$. The profiles indicate that the motor speed will be the limiting factor for small masses; the tip forces induced by the 200kg mass are not sufficient to break the cable tension limits, meaning that the time required to complete the motion will depend mostly on the length of the coasting phase. A faster maximum accleration would cause the tension in cable 3a to fall under the minimum.

The motion planning for a 3000 kg tip mass is shown in Figure 10. One constraint-satisfying solution is $f_c = 0$, and $\frac{d^2\theta_{i,MAX}}{dt^2} = 0.00045 \frac{\text{rad}}{\text{s}^2}$, requiring 124.1 s to complete. For large masses, the cable tension

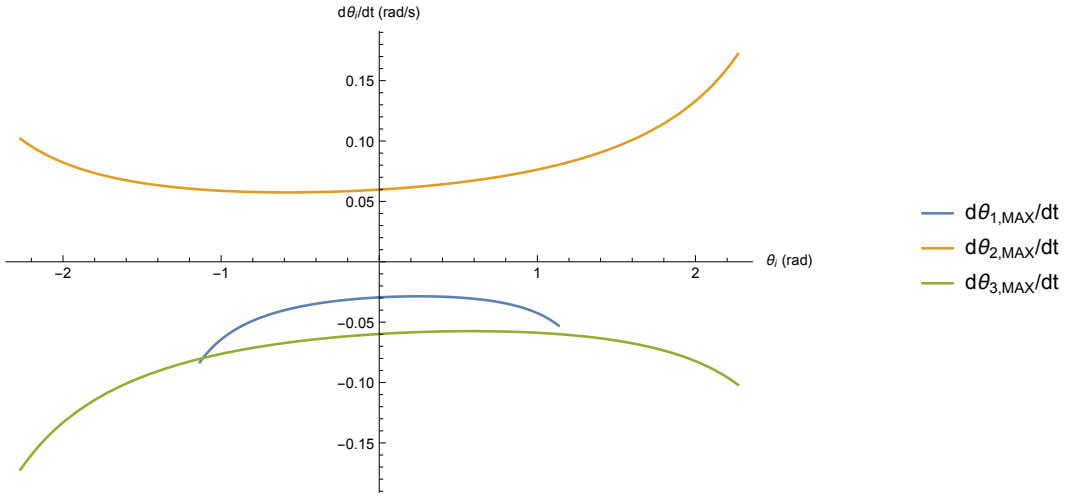


Figure 8. The maximum angular velocities achievable by lengthening the variable tension cable at $\frac{dZ_{i,c,MAX}}{dt}$.

limits will be the driving factor, not the motor speeds, allowing the trapezoid to be compressed to a triangle to minimize the time to completion, eliminating the coasting phase. During the start of deceleration, the moment from the tip mass nearly cancels out the constant tension in cable 1b, reducing the tension in cable 1a almost to the lower limit. Despite eliminating the coasting phase, this maneuver requires triple the amount of time to complete compared to the low mass case.

IV.E. Capturing Objects

The TALISMAN can be used to capture moving objects by executing the latter part of a trapezoid profile, assuming a starting speed greater than 0. To capture an object this way, the velocity of the object at the capture point must be matched by the tip velocity of the TALISMAN at the moment of capture, ensuring a smooth deceleration for the object, in a fashion similar to impedance control.¹⁵ Failure to match velocities could result in sudden changes in tension, resulting in cables going slack or failing.

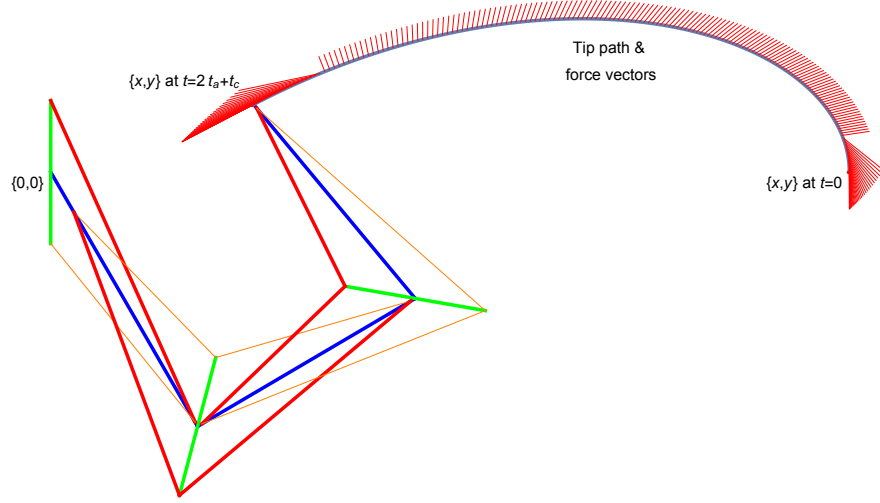
As with the maneuvers in Section IV.D, the results presented here are solutions to the constraint satisfaction problem, attempting to find a near-maximum permissible object starting velocity that the TALISMAN can decelerate to a stop. The object is assumed to be traveling in the positive Y-direction at the tip of the fully extended TALISMAN at $\theta(0) = \{0, 0, 0\}$ rad. To reduce the required deceleration, the stopping distance must be lengthened; setting $\theta(t) = \{\frac{\pi}{3}, \frac{\pi}{3}, \frac{\pi}{3}\}$ rad provides a large deceleration distance without setting the angles to extreme values.

The forces and motor velocities required to decelerate a 200 kg mass at the tip are shown in Figure 11. As with the 200 kg maneuvering case, the driving limit is the motor speed: the motor at joint 1 must be moving at nearly its limit to capture the mass when it is moving at $0.64 \frac{\text{m}}{\text{s}}$. The motors must decelerate at a rate of $0.00075 \frac{\text{rad}}{\text{s}^2}$ to stop the 200 kg mass when starting from an angular velocity of $\frac{d\theta_i}{dt} = 0.029 \frac{\text{rad}}{\text{s}}$.

The forces and motor velocities required to decelerate a 3000 kg mass at the tip are shown in Figure 12. As with the 3000 kg maneuvering case, the driving limit is the cable tension; the tension in cable 1a must be nearly at its lower limit to capture the mass when it is moving at $0.24 \frac{\text{m}}{\text{s}}$. The motors must decelerate at a rate of $0.000105 \frac{\text{rad}}{\text{s}^2}$ to stop the 3000 kg mass when starting from an angular velocity of $\frac{d\theta_i}{dt} = 0.01 \frac{\text{rad}}{\text{s}}$.

IV.F. Maneuver and Capture Discussion

In both the 3000 kg maneuvering and capturing cases, the limit is driven by the tension in cable 1a approaching the minimum. This limit is due to the moment of the tip mass reaction force canceling out the passive tension in cable 1b. Changing the constant tension of cable 1b will enable greater accelerations of large tip masses. Switching to an *active-active* configuration will eliminate the lower tension limit, allowing greater accelerations, and the upper tension limit can be changed by the choice of cable material.



(a) The final pose, with the tip path and relative force directions and magnitudes shown.

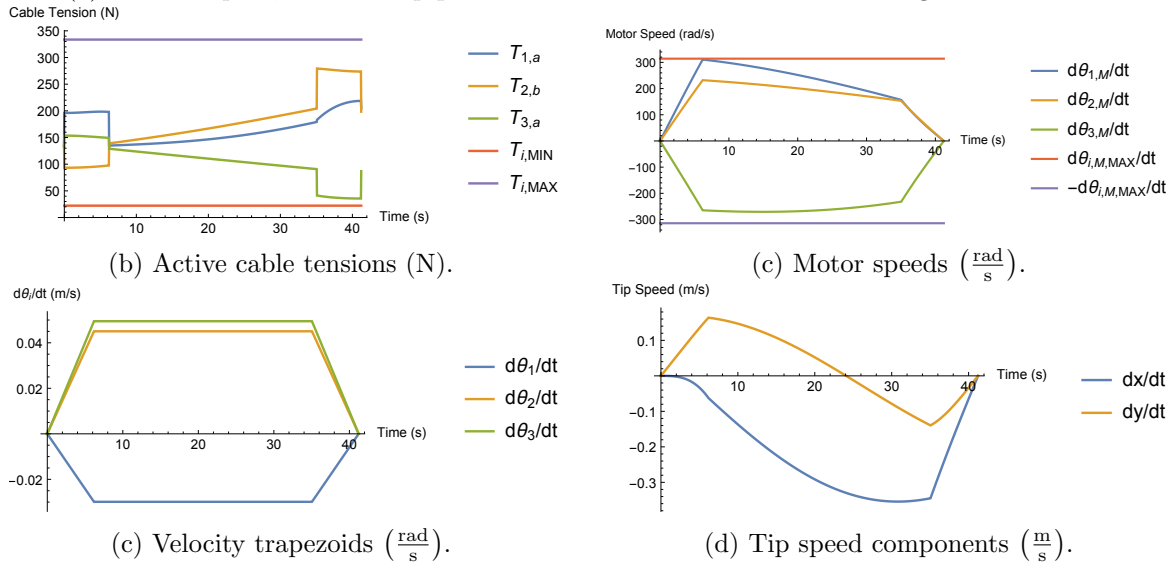


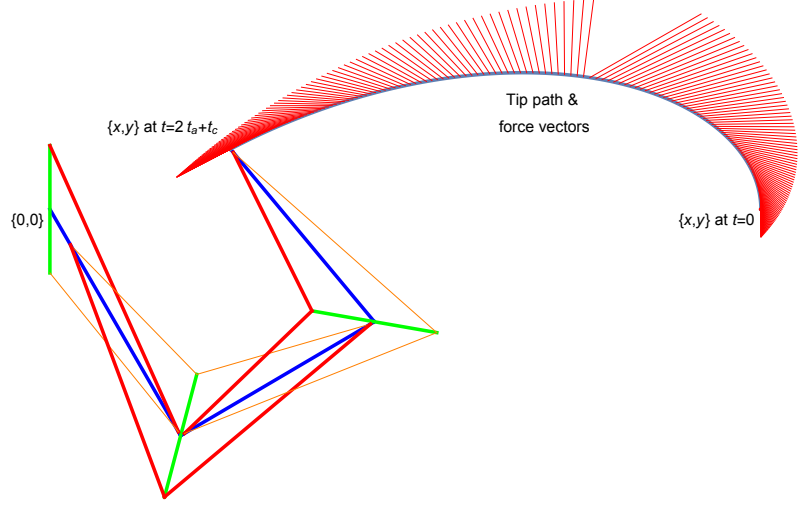
Figure 9. The motions, forces, and speeds required to move a 200 kg mass from the fully extended position to $\{x, y\} = \{3, 1\}$ m while maintaining tension and motor speed limits.

The gear ratio $G = 320$ is also conservative; the allowable capstan force is much larger than the upper tension limit for this prototype. The high gear ratio also limits the angular velocity. Reducing the gear ratio would allow faster TALISMAN motion. However, as the TALISMAN velocity increases, operational risk would likely increase.

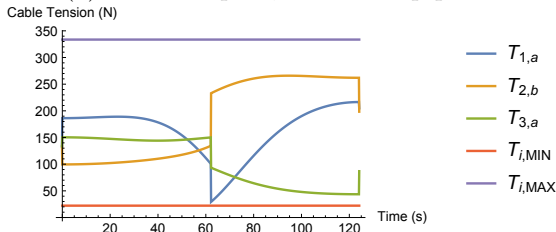
Finally, the tip mass considered here was a point mass, not a rigid body. This limitation can be mitigated by considering the distance between the TALISMAN tip and the center of mass of the object as an extension to the final link distance d_3 , assuming the grip on the object is rigid. If the grip on the object is flexible, there will be additional dynamic motions at the tip, causing a change in the tension profiles. A flexible multibody dynamics model and a dynamic control system will be necessary to accommodate this condition.

V. Satellite Servicing Demonstration and Discussion

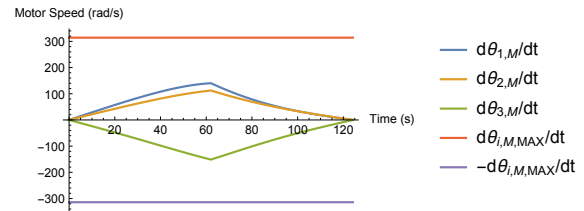
Long-reach robotic manipulation is a critical capability that NASA developed previously with the Shuttle Remote Manipulator System (SRMS) and the Space Station Remote Manipulator System (SSRMS). Having the versatility of a general purpose manipulator successfully enabled a wide variety of operations



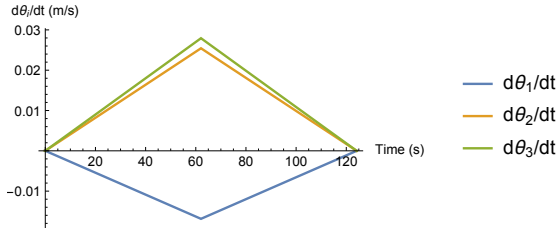
(a) The final pose, with the tip path and relative force directions and magnitudes shown.



(b) Active cable tensions (N).



(c) Motor speeds ($\frac{\text{rad}}{\text{s}}$).



(d) Velocity triangles ($\frac{\text{rad}}{\text{s}}$).

(d) Tip speed components ($\frac{\text{m}}{\text{s}}$).

Figure 10. The motions, forces, and speeds required to move a 3000 kg mass from the fully extended position to $\{x, y\} = \{3, 1\}$ m while maintaining tension and motor speed limits.

such as; satellite servicing, Hubble Space Telescope repair and servicing, extravehicular activity positioning, International Space Station (ISS) assembly, berthing of resupply spacecraft at ISS, and robotic manipulator positioning on ISS to support research and maintenance operations. The TALISMAN not only maintains the versatility of traditional long-reach space manipulators, the TALISMAN increases versatility by providing the capabilities for increased packaging efficiency, increased reach, increased stiffness and reduced mass.

To demonstrate these capabilities, the two operational TALISMAN prototypes were outfitted to perform a satellite servicing demonstration. One TALISMAN was equipped with a passive magnetic gripper, which enabled the grappling of a satellite mockup. The other TALISMAN was equipped with a Robai Cyton Gamma 1500 7-DOF arm, a small robotic arm with a reach of 0.5 m. When used with an end-effector, the TALISMAN becomes a long reach manipulator, with a range of motion of over 10 m, and a high precision capability for localized tasks.

The ability to change end-effectors enables the TALISMAN to perform a large variety of tasks. A servicing spacecraft equipped with one or more TALISMANs and a suite of end-effectors can be used to:

- Capture the spacecraft to be serviced, using a capturing end-effector
- Inspect the spacecraft using an onboard camera at the end-effector

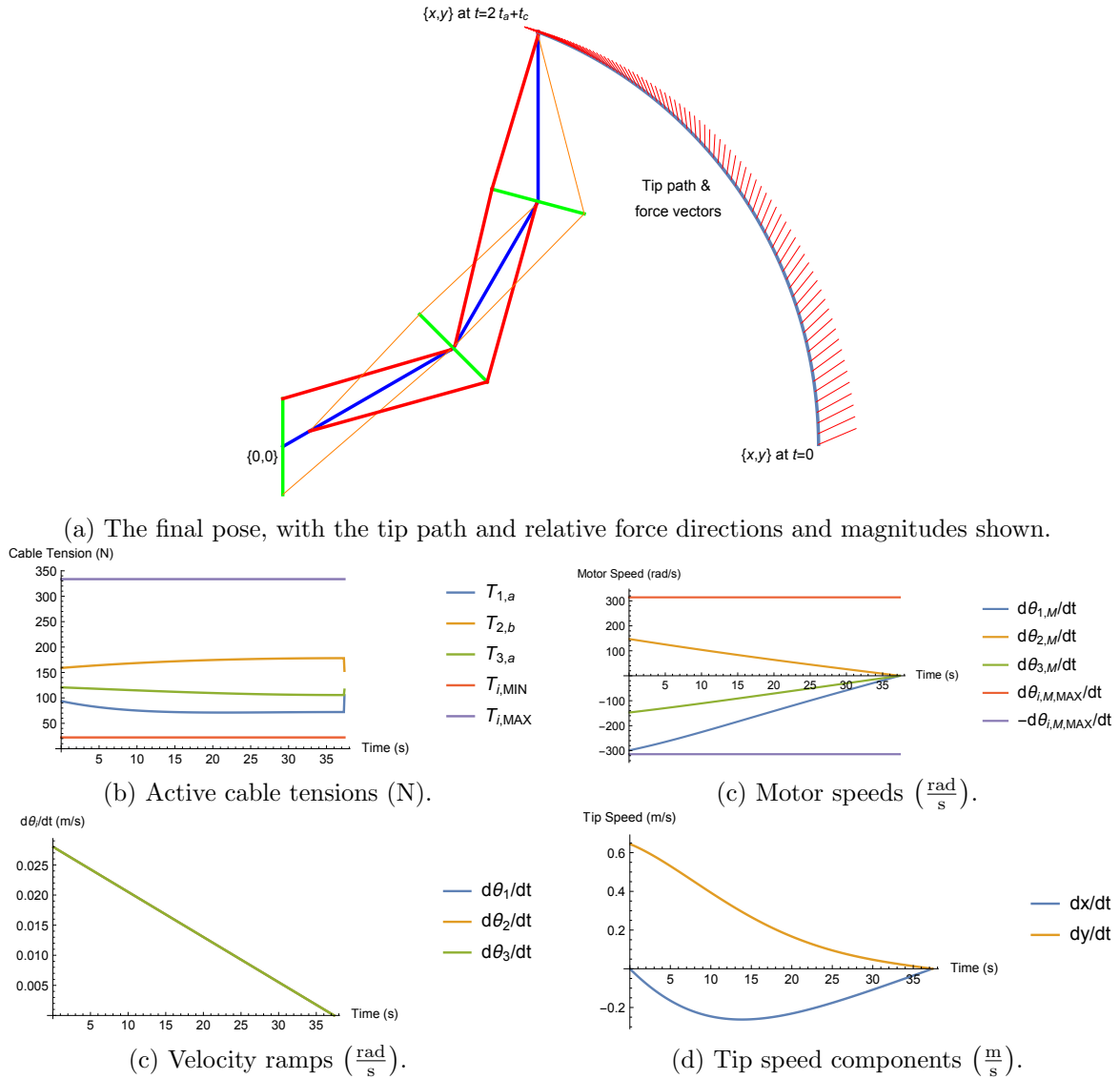


Figure 11. The motions, forces, and speeds required to capture a 200 kg mass, decelerating all joints at a constant rate, while maintaining tension and motor speed limits.

- Perform servicing by using a specialized end-effector to cut, assemble, refuel, or weld.

For this paper, a capturing and inspecting task was performed using a satellite mockup, as shown in Figure 13. The TALISMAN prototypes were teleoperated, simulating a likely scenario for a mission at, or below, geosynchronous orbit. The air bearing floor at Langley Research Center was used to simulate a two-dimensional zero-gravity experiment. In addition to the TALISMAN prototypes resting on air bearings, a satellite mockup was placed on air bearings and allowed to float.

The inspection consisted of the following steps:

- The satellite mockup was set adrift within the workspace of the two TALISMAN prototypes.
- The left arm was teleoperated to capture the mockup, by attaching the magnetic end-effector to a steel plate on the mockup, representing a grasping task.
- Once the residual grasping energy was dissipated, the operator commanded the right arm to the proximal end of the satellite mockup.

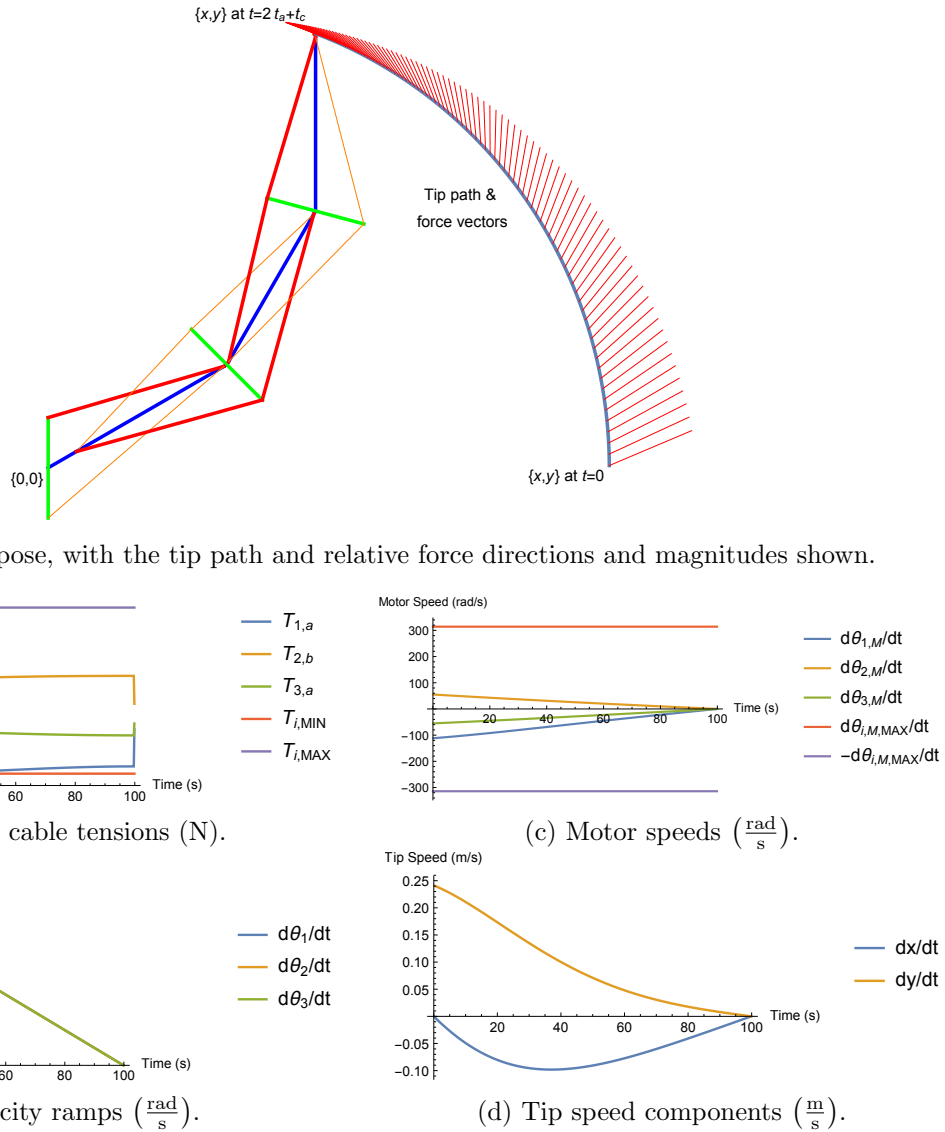


Figure 12. The motions, forces, and speeds required to capture a 3000 kg mass, decelerating all joints at a constant rate, while maintaining tension and motor speed limits.

- The operator commanded the manipulator end-effector to inspect the mockup at a distance of under 20 cm, utilizing the end-effector to inspect vertically with respect to the TALISMAN motion plane.
- The right arm was commanded to move lengthwise along the satellite mockup, allowing the end-effector to perform the previous step. This process was repeated until the operator was able to fully inspect one side of the satellite.

The inspection task shows that the versatility of the TALISMANs themselves, combined with the ability to change end-effectors, can enable a wide range of servicing tasks. However, the demonstration also faced challenges unique to the TALISMAN prototypes. The 30 lb of tension on the passive cables at each joint limits the attainable stiffness, and results in large magnitude, long duration vibrations requiring a few seconds to settle after the grasping task was complete. For applications requiring capturing a rotating or tumbling satellite, *active-active* control will be required. With lower tensions on the cables, passive impedance control may simplify the controls needed to grasp a tumbling satellite. With higher cable tensions, TALISMAN stiffness can be increased, and residual forces from end-effector motion and grasping motions will not result in large deformations in the joints. Although the two-dimensional nature of the demonstration ruled out any exploration of the effects of torsion or out-of-plane stresses on the TALISMAN prototypes, their design

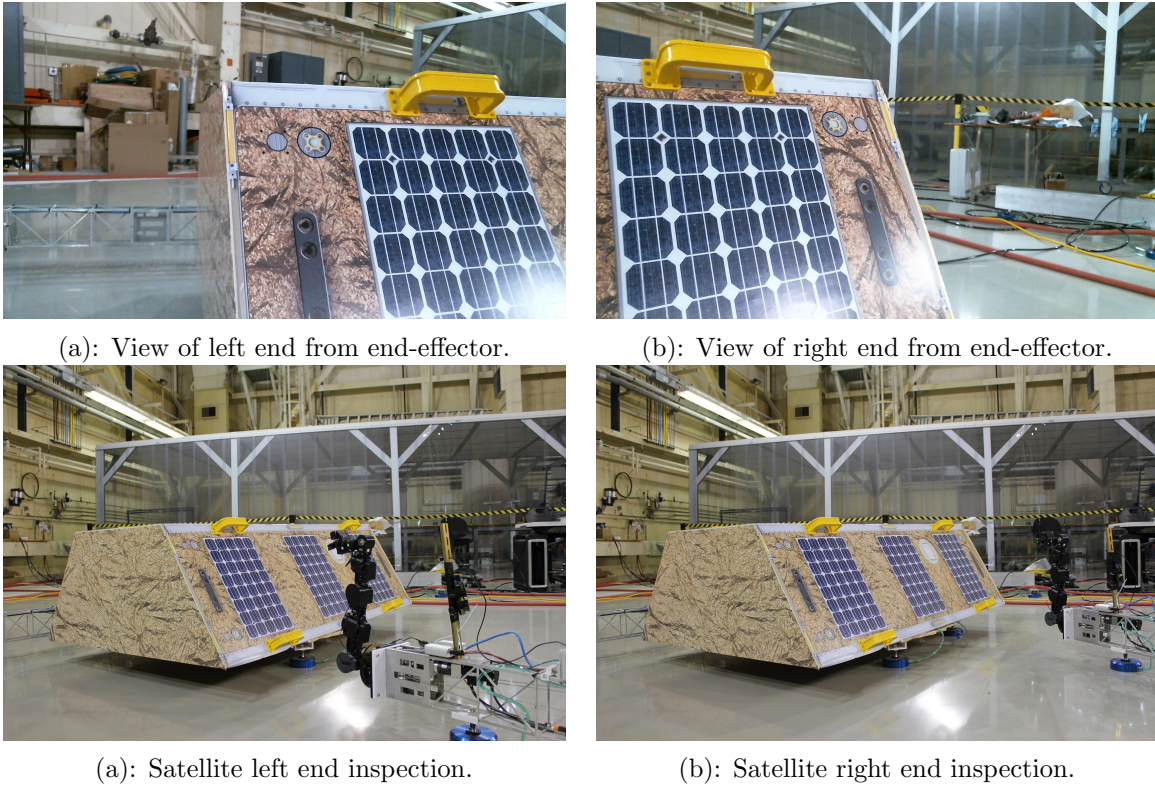


Figure 13. The end-effector manipulator’s onboard camera inspects the satellite mockup.

accounts for out-of-plane forces.

VI. Potential Avenues for Improvement

Control system updates are underway. The control system, as currently implemented, needs to be modified for additional links. The simplest method to do so would be to extend the current method; for a robot with N links, the first $N - 2$ link angles and angular velocities are free parameters, and the final two links are modified. As an alternative, the Moore-Penrose Pseudoinverse¹⁶ Jacobian could replace the inverse Jacobian, and provides a convenient way to calculate the full set of angular velocities that match a desired endpoint velocity (including an endpoint velocity of 0, allowing the robot to move its joints within its null space). The pseudoinverse allows joint motions to be calculated with constraints, such as self-intersection and intersection with other bodies, or to minimize a metric such as energy expenditure. This can be paired with a path planning algorithm such as Rapidly-exploring Rapid Trees⁶ to find feasible routes with a large number and variety of constraints.

Additional sensors will be implemented to complement the current suite of sensors. Work has already begun on implementing a computer vision system to augment the joint angle measurements and to enable visual servoing.¹⁷ Along with the sensors, higher fidelity estimation algorithms will be required, such as particle filters or extended Kalman filters,¹⁸ for which design and simulations are currently ongoing.

TALISMAN operational performance will benefit from increased damping. The simplest method to implement would be a passive damping system. However, with an *active-active* configuration, active damping can be achieved by controlling the tension in the cables. The PID controller which was implemented addresses this problem, but must be tuned manually. A replacement control system could be a nonlinear one,¹⁹ but linearizable around the set point for small perturbations, enabling the use of Linear-quadratic-Gaussian control,⁷ combining an optimal controller with optimal estimation from a Kalman filter.

Finally, it is also planned to use the current prototype TALISMAN to perform additional higher fidelity operational demonstrations. For example, the gripper at the tip of the end-effector can be used to perform a screwing/unscrewing task, enabling assembly and disassembly.

VII. Concluding Remarks

The control system of an 11.8 m, 3-link TALISMAN prototype, and a successful demonstration of a satellite inspection task requiring one TALISMAN to grasp a satellite mockup and the other to inspect it using a robotic end-effector, are described in this paper. The control system implemented on the current prototype enables the maneuvering of small (200 kg) and large (3000 kg) masses from rest, and also allows the capture of moving objects, such as satellites. Descriptions of how such maneuvers may be planned and executed, as well as potential avenues for improvement of the control system, are described in this paper.

The *active-passive* configuration presented in this paper was convenient for prototype cost reduction, but is not recommended for satellite servicing missions. The use of the passive cables imposes hard limits in cases where the constant tension has to balance out a moment induced by a tip force; such as the 3000 kg maneuvering and capturing tasks. For a full antagonistic *active-active* TALISMAN with four motors and four tunable tension cables per joint, the lower tension limit can be eliminated.

References

- ¹Hunter, J. A., Ussher, T. H., and Gossain, D. M., "Structural Dynamic Design Considerations of the Shuttle Remote Manipulator System," *Proceedings of the 23rd AIAA Structural Dynamics and Materials Conference*, No. 82-0762, New Orleans, USA, May 1982.
- ²McGregor, R. and Oshinowo, L., "Flight 6A: Deployment and Checkout of the Space Station Remote Manipulator System (SSRMS)," *Proceedings of the 6th International Symposium on Artificial Intelligence, Robotics and Automation in Space (i-SAIRAS)*, Montreal, Canada, June 2001.
- ³Doggett, W. R., Dorsey, J. T., Jones, T. C., and King, B., "Development of a Tendon-Actuated Lightweight In-Space MANipulator (TALISMAN)," *Proceedings of the 42nd Aerospace Mechanisms Symposium*, NASA Goddard Space Flight Center, Greenbelt, USA, May 2014.
- ⁴Dorsey, J. T., Doggett, W. R., Jones, T. C., and King, B., "Application of a Novel Long-Reach Manipulator Concept to Asteroid Redirect Missions," *Proceedings of the AIAA Science and Technology Forum*, Kissimmee, USA, January 2015.
- ⁵Doggett, W. R., Dorsey, J. T., Collins, T., King, B., and Mikulas, M., "A Versatile Lifting Device for Lunar Surface Payload Handling, Inspection & Regolith Transport Operations," *Space Technology and Applications International Forum*, Albuquerque, USA, February 2008.
- ⁶Choset, H., Lynch, K. M., Hutchinson, S., Kantor, G., Burgard, W., Kavraki, L. E., and Thrun, S., *Principles of Robot Motion: Theory, Algorithms, and Implementations*, MIT Press, 2005.
- ⁷Hespanha, J. P., *Linear Systems Theory*, Princeton University Press, 2009.
- ⁸Anon., "Beckhoff Automation GmbH and Co. KG," Accessed: 2015-07-13, <http://www.beckhoff.com>.
- ⁹Altenbuchner, C., Dorsey, J. T., and Jones, T. C., "Flexible Multi- Body Dynamic Modeling of Tendon-Actuated Lightweight In- Space Manipulator (TALISMAN)," *Proceedings of the AIAA SPACE Conference*, Pasadena, USA, September 2015 (In Preparation).
- ¹⁰Anon., "Contelec Vert-X," Accessed: 2015-07-13, <http://www.contelec.ch/en/produkte.html?action=list&typ=Vert-XXE>.
- ¹¹Anon., "Load Cells — Toledo Integrated Systems," Accessed: 2015-07-13, http://www.toledointegratedsystems.com/products/load_cells/index.php.
- ¹²Anon., "Robai Cyton Gamma 1500," Accessed: 2015-07-13, <http://www.robai.com/robots/robot/cyton-gamma-1500/>.
- ¹³Anon., "Ametek Spring B Motor Assemblies," Accessed: 2015-07-13, <http://www.ametekhunterspring.com/Products/Mechanical-Reels/Spring-B-Motor-Assembly.aspx>.
- ¹⁴Bauchau, O. A., *Flexible Multibody Dynamics*, Vol. 176, Springer Science & Business Media, 2010.
- ¹⁵Hogan, N., "Impedance Control: An Approach to Manipulation: Part IIIImplementation," *Journal of Dynamic Systems, Measurement, and Control*, Vol. 107, No. 1, 1985, pp. 8–16.
- ¹⁶Ben-Israel, A. and Greville, T. N. E., *Generalized Inverses: Theory and Applications*, Vol. 15, Springer Science & Business Media, 2003.
- ¹⁷Corke, P., *Robotics, Vision and Control: Fundamental Algorithms in MATLAB*, Vol. 73, Springer Science & Business Media, 2011.
- ¹⁸Thrun, S., Burgard, W., and Fox, D., *Probabilistic Robotics*, MIT Press, 2005.
- ¹⁹Khalil, H. K., *Nonlinear Systems: Third Edition*, Vol. 3, Prentice Hall, 2002.